Electronic structure of InAs/GaAs self-assembled quantum dots

M. A. Cusack, P. R. Briddon, and M. Jaros
Department of Physics, The University of Newcastle upon Tyne, Newcastle upon Tyne, United Kingdom
(Received 23 April 1996)

The electronic properties of the self-assembled InAs/GaAs quantum dots are investigated theoretically. In our calculation the microscopic distribution of the strain, valence-band mixing, and the shape of the conduction band of InAs with strain are fully taken into account. New states are brought to light and their status in the framework of established approximate models of the electronic structure is critically examined. [S0163-1829(96)50328-0]

Recent studies[1–4] have shown that it is possible to attain three-dimensional (3D) confinement of charge within strained islands of InAs that form on the surface of GaAs during the Stranski-Krastanow growth method. This growth mode begins with an initial molecular-beam-epitaxy layer deposition of InAs on a GaAs substrate. After a critical thickness of 1.7 ML is reached[6] islands of InAs with a pyramidal geometry form spontaneously and a thin wetting layer is left under the islands. Fabrication concludes with the capping of the quantum dot island with a layer of the substrate material. By this method defect-free quantum dots with sizes ≈ 120 Å can be constructed with no need for processing by lithography and etching. It has been demonstrated[5] that the island sizes and areal densities can be controlled by varying growth parameters such as the thickness of the initial two-dimensional layer deposition, and the growth rate.

The first theoretical study of the electronic properties of these structures[7] used the single-band effective-mass theory to calculate the energy levels and wave functions in InAs/GaAs cone-shaped quantum dots. The strain was taken to be a constant in the InAs material and zero in the surrounding GaAs barrier. More recently, the single-band theory was applied to InAs/GaAs dots with a more realistic pyramidal geometry.[8] There the variation of the strain in and around the InAs island was determined using elastic continuum theory, in which the atomic nature of the constituent materials was neglected. Both approaches neglected valence-band mixing, and the strain dependence of the effective masses.

In this paper we present a calculation of the electronic structure of InAs/GaAs quantum dots that includes the microscopic details of the strain and the mixing between the light-hole (lh) and heavy-hole (hh) bulk bands, and accounts for the change in the effective masses due to strain. We employed a valence force field method[9] to determine the structure and the variation of strain, and a multiband effective-mass method to calculate the confined levels.

The atomic positions in four strained InAs/GaAs pyramidal quantum dot systems consisting of 2×10^6 atoms (Fig. 1) have been determined. The dimensions of each dot are given in Table I. Each pyramid lies on a 1.5-ML InAs layer. The bulk lattice constant of each structure was made equal to that of GaAs (5.65 Å) and their constituent atoms relaxed into a minimum energy configuration within the framework of the valence force field model. The potential included five terms for each material describing bond-bending and bond-stretching interactions and the couplings between bending and stretching in adjacent bonds and angles. Force constants were obtained by fitting to the phonon spectra of InAs and GaAs. In particular, it was verified that the low-frequency part of the spectrum was well reproduced and agreed with the values predicted from the elastic constants of the material. This was important as it is primarily the longer-wavelength variation in strain that is extracted from this part of the calculation and used in the electronic structure determination described below. It should of course be noted that the accuracy of the valence force field model goes beyond classical elasticity theory and should also give a reasonable description of relaxation on an atomic scale.

Bulk unit cells in each structure were assigned a strain tensor on the basis of the displacement of the atoms from their equilibrium positions. This approach provided values of the six independent nonzero strain tensor components for each bulk unit cell except those at the interface. Figure 2(a) shows the strain tensor components ϵ_{xx} and ϵ_{zz} for structure 4 in Table I plotted with position along the z axis in Fig. 1. By symmetry $\epsilon_{yy}=\epsilon_{xx}$. The shear strain components, ϵ_{xy}, ϵ_{xz}, and ϵ_{yz}, are negligible in the dot and barrier although they could be appreciable at the interface.[8]

The hydrostatic and biaxial components of the strain, defined as

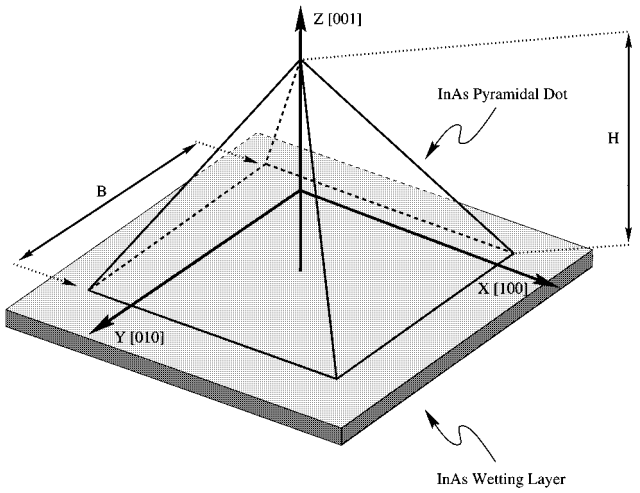

FIG. 1. Schematic diagram of an InAs pyramidal quantum dot and InAs wetting layer together with the axes referred to in the text.

TABLE I. Dimensions and fundamental transition energy of the four structures studied.

Structure	B (Å)	H (Å)	$C1 \rightarrow V1$ (eV)
1	57	28	1.43
2	79	40	1.33
3	102	51	1.23
4	124	62	1.11

$$\epsilon_h = \epsilon_{xx} + \epsilon_{yy} + \epsilon_{zz} \quad \text{and} \quad \epsilon_b = 2\epsilon_{zz} - \epsilon_{xx} - \epsilon_{yy}, \tag{1}$$

are plotted with position along the z axis in Fig. 2(b) for structure 4. The hydrostatic strain is compressive in both the dot and the surrounding barrier material. The biaxial strain, which can be thought to consist of a hydrostatic strain plus a uniaxial strain, tends to be negative in the barrier and positive in the dot.

To calculate the energy levels and electron (or hole) wave functions we use the multiband effective-mass theory. For simplicity, we assume that the conduction and valence bands are decoupled. The general solutions for the electron states are

$$\psi_n^c(x,y,z) = u^c \phi_n^c(x,y,z), \tag{2}$$

where u^c is a bulk band-edge Bloch function and ϕ_n^c is an envelope function satisfying the simple single-band Schrödinger equation,

$$[-(\hbar^2/2m^*)\nabla^2 + V(x,y,z)]\phi(x,y,z) = E\phi(x,y,z), \tag{3}$$

in which m^* is the isotropic effective mass and $V(x,y,z)$ is the three-dimensional confining potential. Equation (3) is solved for the eigenvalues and eigenfunctions of the system by invoking periodic boundary conditions, expanding ϕ in terms of normalized plane-wave states, and diagonalizing the resultant matrix. To ensure adequate convergence approximately 1000 plane-wave states were used in our expansion. The attraction of this approach is that there is no need to explicitly match wave functions across a boundary between the barrier and dot materials; the method is thus easily applicable to an arbitrary confining potential. The boundary conditions are that the states in neighboring quantum dots do not significantly overlap.

The valence-band states are defined by solutions of the four-band Schrödinger equation, which in bulk semiconductors has the form

$$\begin{pmatrix} H_{\rm hh} & -c & -b & 0 \\ -c^* & H_{\rm lh} & 0 & b \\ -b^* & 0 & H_{\rm lh} & -c \\ 0 & b^* & -c^* & H_{\rm hh} \end{pmatrix} \begin{pmatrix} \phi_{3/2,+3/2} \\ \phi_{3/2,-1/2} \\ \phi_{3/2,+1/2} \\ \phi_{3/2,-3/2} \end{pmatrix} = E \begin{pmatrix} \phi_{3/2,+3/2} \\ \phi_{3/2,-1/2} \\ \phi_{3/2,+1/2} \\ \phi_{3/2,-3/2} \end{pmatrix}. \tag{4}$$

The elements in the Hamiltonian are given by

$$H_{\rm hh} = (-\hbar^2/2m_0)[(k_x^2+k_y^2)(\gamma_1+\gamma_2) + k_z^2(\gamma_1 - 2\gamma_2)],$$

$$H_{\rm lh} = (-\hbar^2/2m_0)[(k_x^2+k_y^2)(\gamma_1-\gamma_2) + k_2^2(\gamma_1 + 2\gamma_2)],$$

$$c = (\sqrt{3}\hbar^2/2m_0)[\gamma_2(k_x^2 - k_y^2) - 2i\gamma_3 k_x k_y],$$

$$b = (\sqrt{3}\hbar^2/m_0)(k_x - ik_y)\gamma_3 k_z. \tag{5}$$

Here $\gamma_1, \gamma_2, \gamma_3$ are the Kohn-Luttinger parameters. In the case of the quantum dot, the equation becomes

$$[H + V(x,y,z)]\phi^v(x,y,z) = E\phi^v(x,y,z), \tag{6}$$

where the confining potential $V(x,y,z)$ is added to the diagonal elements of the 4×4 matrix. Since, for the problem of 3D quantum confinement, k_x, k_y, k_z are no longer good quantum numbers, we replace them in Eq. (5) with the operators

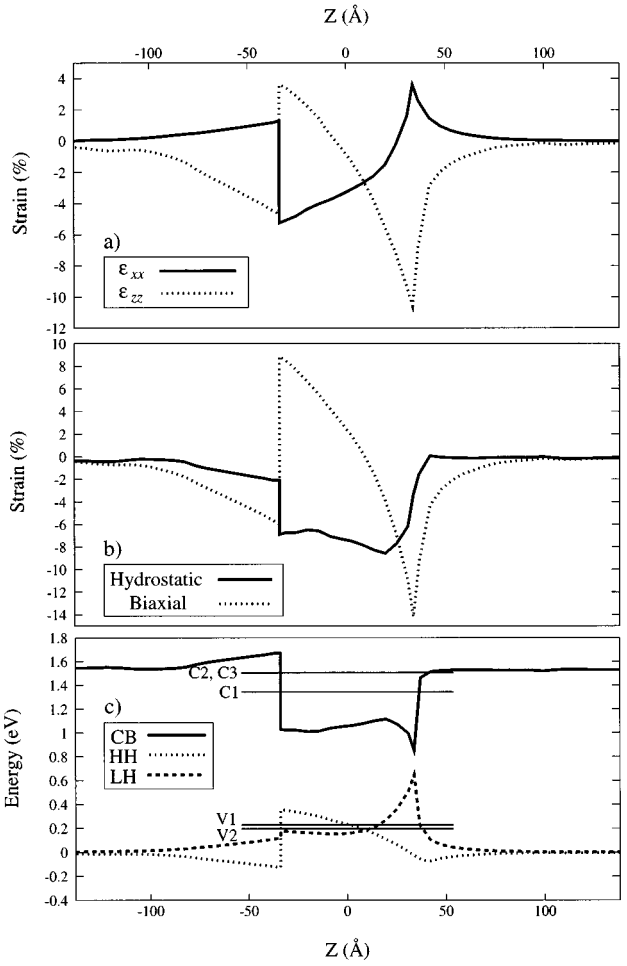

FIG. 2. (a) Strain tensor components ϵ_{xx} and ϵ_{zz} for structure 4 in Table I plotted along the z axis. (b) Hydrostatic and biaxial components of the strain for structure 4 in Table I plotted along the z axis. (c) Ground and first excited electron and hole levels ($C1$, $C2$, $C3$, $V1$, $V2$) in structure 4 superimposed upon the electron, heavy-hole, and light-hole potential profiles.

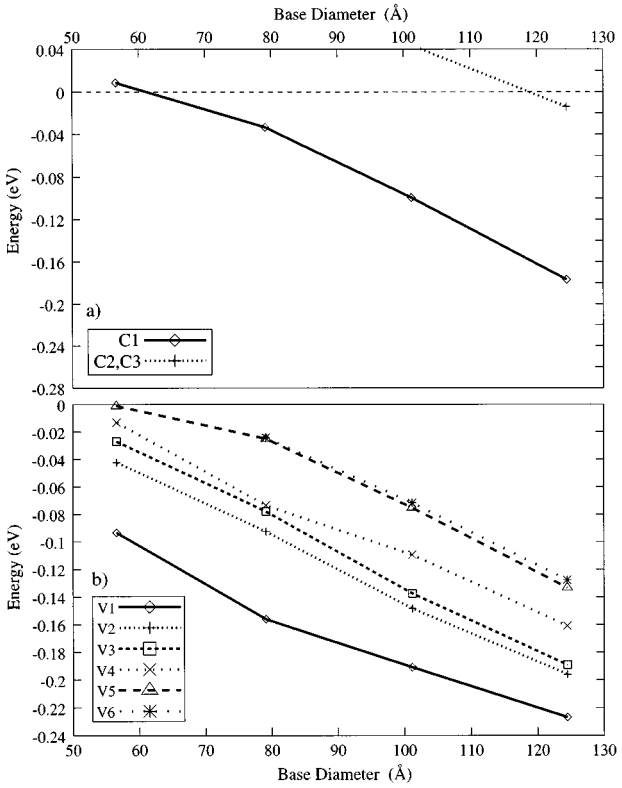

FIG. 3. (a) Electron and (b) hole quantum dot energy levels displayed as a function of dot base size.

$$k_x = -i\hbar\,\partial/\partial x\,,\quad k_y = -i\hbar\,\partial/\partial y\,,\quad k_z = -i\hbar\,\partial/\partial z\,. \qquad (7)$$

Equation (6) is solved using an expansion in plane waves, and the valence-band wave functions are given by

$$\psi_n^v(x,y,z) = \sum_{\nu=1}^{4} u^\nu \phi_n^\nu(x,y,z), \qquad (8)$$

where u^ν are the $J=3/2$ angular momentum states.

In the dot material, the compressive stress alters the curvature of the bulk bands causing the effective masses to differ from those of unstrained InAs. In our calculation we used the effective masses of bulk InAs under the average hydrostatic strain present in the dot material. These values were obtained by performing semiempirical pseudopotential band-structure calculations[10] for the conduction-band → valence-band momentum matrix elements of InAs under pressure. In the conduction band, these calculations yield a value for the effective mass of $0.04m_e$ compared to the value for unstrained InAs of $0.023m_e$. The same trend is recovered in *ab initio* local-density calculations. However, the *ab initio* mass in InAs is too high and the empirical pseudopotential result is more representative.

In the absence of strain effects, the confining potential for an electron (hole) is a square well formed by the difference in the absolute energy of the conduction (valence) -band edges in InAs and GaAs given by Ref. 11. In each conventional cubic unit cell, the confining potential for each carrier type is shifted due to the strain. Since the strain varies from cell to cell, the confining potentials will also vary from cell to cell. Furthermore, degeneracies in the valence-band edge

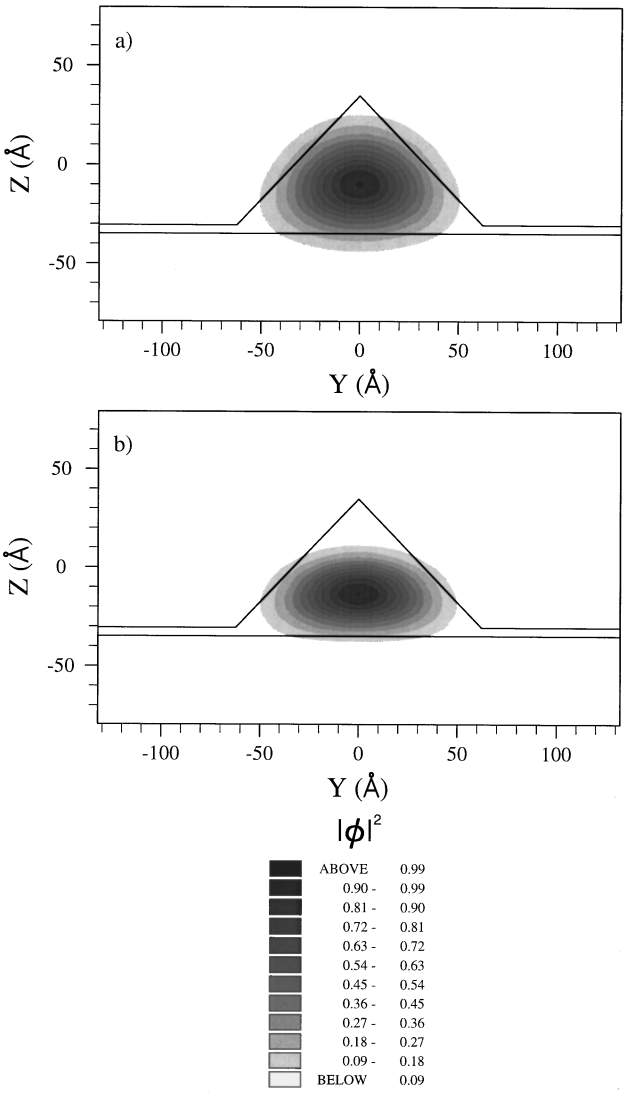

FIG. 4. Plots of $|\phi|^2$ for structure 4 in Table I through the yz plane for (a) the ground electron level and (b) the ground hole level.

will be lifted due to deviations of the unit cells from cubic symmetry. For each unit cell, the strain-induced shifts to the confining potentials are obtained by diagonalizing the 8×8 strain Hamiltonian matrix in Ref. 12. Hence, the confining potentials including the effects of strain are piecewise continuous functions of position.

Figure 2(c) shows the confining potentials for electrons, heavy holes, and light holes along the z axis for structure 4. The energies are relative to the unstrained GaAs valence-band edge. The splitoff band edge is far in energy from the heavy-hole and light-hole band edges and plays no part in our calculation. Included in Fig. 2(c) are the ground and first excited electron and hole energy levels for the quantum dot, generated by our calculation.

The compressive strain in the barrier shifts the GaAs conduction-band edge slightly above the unstrained level (at 1.519 eV). From Fig. 2(c) it is clear that the light-hole band edge is higher in energy than the heavy-hole band edge in the barrier, and towards the apex of the pyramid. The heavy-hole band is the uppermost band at the base of the pyramid. The direction and magnitude of the splitting of the light- and

heavy-hole bands—in the absence of appreciable shear strain components—is dependent solely on the magnitude and sign of the biaxial strain, ϵ_b [see Fig. 2(b)]. In those regions of the structure where the biaxial strain is negative the light-hole band will be shifted upwards in energy and the heavy-hole band downwards; in those regions where the biaxial strain is positive, the heavy-hole band will be uppermost. When the biaxial strain function is zero, the light- and heavy-hole bands will be degenerate.

In Fig. 3 we present the electron and hole energy levels as a function of base diameter given by our method. The electron (hole) states are plotted relative to the unstrained conduction (valence) -band edge in GaAs. For dot base diameters smaller than approximately 60 Å we predict no bound-electron states. This number increases to three for structures larger than 120 Å. In the valence band there are many confined hole states. This is due to the larger effective mass associated with these carriers, and to the nature of the light-hole confinement potential the smoothly varying form of which leads to a quasicontinuum of tenuously bound states. Due to the C_{4v} symmetry of the pyramidal dot we would have expected the first and second excited hole states to be degenerate. This is true for the electron levels. However, in the valence band the first and second excited hole levels are split due to mixing between different bulk states.

In Fig. 4(a) the charge density of the $C1$ state for structure 4 is plotted in the yz plane through the pyramid and wetting layer. The relatively isotropic character of the confining potential for electrons coupled with the small effective mass results in a state that permeates throughout the dot and penetrates the sides of the pyramid. Charge does not significantly sample the apex or the base corners of the pyramid. In Fig. 4(b) we show the charge density of the $V1$ state plotted in the yz plane. Unlike the ground conduction state, the ground hole state is confined to the base of the dot due to the larger effective mass, and the anisotropic nature of the heavy-hole confining potential.

The calculated energies for the $C1 \rightarrow V1$ transition in each structure are given in the fourth column of Table I. The fundamental transition energy of 1.11 eV for structure 4 is in excellent agreement with the photoluminescence value of 1.1 eV for a similar-sized structure.[4] The energy splitting between the ground and first excited hole state of 30 meV is in good agreement with a very recent experimental study[13] of the sublevel structure that measured a difference of ≈ 27 meV. However, this work also shows that a larger number of conduction states than predicted by this study and previous calculations[7,8] contribute effectively to optical spectra. For example, in our calculation only one excited state exists at a much higher energy. Furthermore, the observed transition energies form a sequence resembling that arising from confinement in parabolic wells. Our evaluation of the confining semiclassical potential that determines the electronic structure in the particle in a box approximation shows that, at least for dots of ideal or near ideal geometry, the effect of strain does not lead to confining potentials of parabolic form. Also, the charge of the states in question is well confined in the dot so that reexamination of any subtle discrepancies arising from the possible choice of boundary conditions for integration of the Schrödinger equation cannot help. It would appear that a fundamentally more sophisticated Hamiltonian consistent with the confining potentials obtained in our valence force calculation is needed to account for the richness of the observed spectra.

In summary, we calculated the energy levels and wave functions of InAs/GaAs self-organized quantum dots of differing sizes. We took into account the strain modification to the confinement potential, valence-band mixing, and the conduction-band mass in the InAs dot and the surrounding GaAs barrier. We showed that the geometry of the system coupled with the inhomogeneous strain confines the ground electron and hole states to the base of the pyramidal dot. The calculated fundamental transition energy and the valence sublevel structure agree very well with the available experimental data. However, in the conduction band very recent experimental studies indicate that many more conduction states may be involved in the construction of optical spectra than predicted here.

We should like to thank Professor P. M. Petroff for providing us with recent experimental results prior to publication, and to the EPSRC and the Office of Naval Research for financial support.

[1] J. M. Moison, F. Houzay, F. Barthe, L. Leprince, E. André, and O. Vatel, Appl. Phys. Lett. **64**, 196 (1994).
[2] J.-Y. Marzin, J.-M. Gérard, A. Izraël, D. Barrier, and G. Bastard, Phys. Rev. Lett. **73**, 716 (1994).
[3] G. Medeiros-Ribeiro, D. Leonard, and P. M. Petroff, Appl. Phys. Lett. **66**, 1767 (1995).
[4] M. Grundmann, J. Christen, N. N. Lendentsov, J. Böhrer, D. Bimberg, S. S. Ruvimov, P. Werner, U. Richter, U. Gösele, J. Heydenreich, V. M. Ustinov, A. Yu. Egorov, A. E. Zhukov, P. S. Kop'ev, and Zh. I. Alferov, Phys. Rev. Lett. **74**, 4043 (1995).
[5] G. S. Solomon, J. A. Trezza, and J. S. Harris, Jr., Appl. Phys. Lett. **66**, 3161 (1995).
[6] D. Leonard, K. Pond, and P. M. Petroff, Phys. Rev. B **50**, 11 687 (1994).
[7] J.-Y. Marzin and G. Bastard, Solid State Commun. **92**, 437 (1994).
[8] M. Grundmann, O. Stier, and D. Bimberg, Phys. Rev. B **52**, 11 969 (1995).
[9] R. M. Martin, Phys. Rev. B **1**, 4005 (1969).
[10] D. Ninno, M. A. Gell, and M. Jaros, J. Phys. C **19**, 3895 (1985).
[11] C. G. Van der Walle, Phys. Rev. B **39**, 1871 (1989).
[12] F. H. Pollak, Semicond. Semimet. **32**, 17 (1990).
[13] K. H. Schmidt, G. Medeiros-Ribeiro, M. Oestreich, and P. M. Petroff, Phys. Rev. B (to be published).